3.5.4 ICRS Centre

Paris Observatory ICRS Center activities during 2016

Analysis of recent VLBI catalogs

Data sets

Six catalogs were submitted respectively by the Italian Space Agency (ASI; asi2016a), Geoscience Australia (aus2016a; aus2016b), the Federal Agency for Cartography and Geodesy (BKG Leipzig) and Institute of Geodesy and Geoinformation of the University of Bonn (IGGB; bkg2016a), and the US Naval Observatory (usn2016a). All these catalogs provide right ascension (α) and declination (δ) of extragalactic radio sources, as well as their respective uncertainties, the correlation coefficient between α and δ, and the number of sessions and delays. Note that bkg2016a and usn2016a catalogs were produced with the same geodetic VLBI analysis software package SOLVE developed at NASA GSFC. Solutions aus2016a and aus2016b were produced with OCCAM. The catalogs are displayed in Fig. 1 with color codes following the formal error on the source position.

Table 1: *Number of sources (total and in common with ICRF2 and the Gaia DR1 catalog) and median error (in microarc second). Values for right ascension, referred to as RA*, are corrected from the cosine of the declination.*

	No Sources			Median Err	
	Total	ICRF2	Gaia	RA*	Dec
asi2016a	1368	1339	958	56	92
aus2016a	3900	3284	2106	442	728
aus2016b	3917	3290	2109	432	700
bkg2016a	3507	3122	2029	234	428
usn2016a	4129	3412	2191	213	364

Table 1 displays the total number of sources of each catalog, as well as the number of sources in common with the ICRF2 (Fey et al. 2015) and the Gaia DR1 auxiliary solution (Mignard et al. 2016). Table 1 also reports the median error and reveals an error in declination larger than in right ascension by a factor of $\sim$1.5. The error is substantially smaller for SOLVE solutions compared to OCCAM, except the solution asi2016a whose smaller error likely originates in the fact that the solution considered a relatively small number of well observed sources with low positional standard error.

Figure 2 illustrates how the overall formal error, defined as the square root of $\sigma\alpha\cos\delta 2+\sigma\delta 2+c\sigma\alpha\cos\delta\sigma\alpha\delta$ where σ is the formal error listed in the catalogs and c is the correlation coefficient between estimates

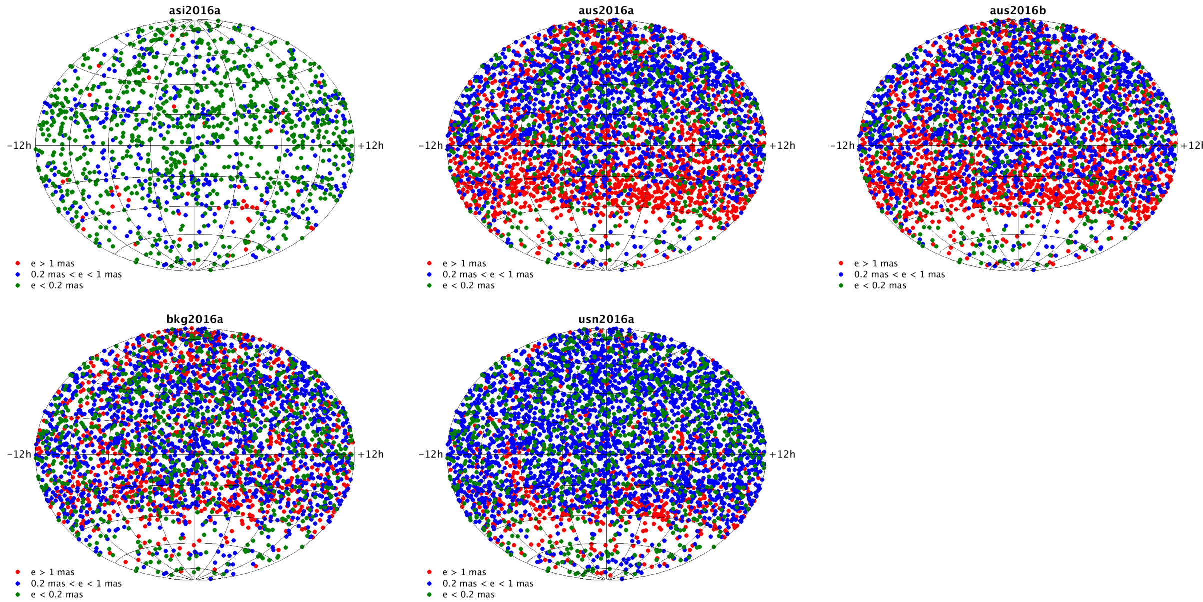

Fig. 1: *The source distribution on the sky.*

of α and δ as provided in the catalogs, varies with the number N of observations. The figure for aus2016b clearly shows that some sources have underestimated formal errors likely due to an overconstrained solution. (As stated in the technical document delivered with the catalog, a strong no-net rotation condition was imposed to these sources. A similar fact was pointed for solution aus2015a in the 2014 IERS Annual Report.) The formal error of the same sources in solution aus2016a, in which the no-net rotation condition is less severe, appears to be at a level comparable to other sources.

Frame deformation

We evaluate the consistency of the submitted catalogs with the ICRF2 and Gaia DR1 by modeling the coordinate difference (in the sense catalog minus reference) by a 16-parameter transformation including three rotations, a glide (three parameters), and a quadrupolar deformation (e.g., Mignard and Klioner 2012).

$$\begin{aligned}
\Delta\alpha\cos\delta &= R_1\cos\alpha\sin\delta + R_2\sin\alpha\sin\delta - R_3\cos\delta - D_1\sin\alpha + D_2\cos\alpha + a_{20}^{M}\sin 2\delta \\
&+ \left(a_{21}^{E,\mathrm{Re}}\sin\alpha + a_{21}^{E,\mathrm{Im}}\cos\alpha\right)\sin\delta - \left(a_{21}^{M,\mathrm{Re}}\cos\alpha - a_{21}^{M,\mathrm{Im}}\sin\alpha\right)\cos 2\delta \\
&- 2\left(a_{22}^{E,\mathrm{Re}}\sin 2\alpha + a_{22}^{E,\mathrm{Im}}\cos 2\alpha\right)\cos\delta - \left(a_{22}^{M,\mathrm{Re}}\cos 2\alpha - a_{22}^{M,\mathrm{Im}}\sin 2\alpha\right)\sin 2\delta, \\
\Delta\delta &= -R_1\sin\alpha + R_2\cos\alpha - D_1\cos\alpha\sin\delta - D_2\sin\alpha\sin\delta + D_3\cos\delta + a_{20}^{E}\sin 2\delta \\
&- \left(a_{21}^{E,\mathrm{Re}}\cos\alpha - a_{21}^{E,\mathrm{Im}}\sin\alpha\right)\cos 2\delta - \left(a_{21}^{M,\mathrm{Re}}\sin\alpha + a_{21}^{M,\mathrm{Im}}\cos\alpha\right)\sin\delta \\
&- \left(a_{22}^{E,\mathrm{Re}}\cos 2\alpha - a_{22}^{E,\mathrm{Im}}\sin 2\alpha\right)\sin 2\delta + 2\left(a_{22}^{M,\mathrm{Re}}\sin 2\alpha + a_{22}^{M,\mathrm{Im}}\cos 2\alpha\right)\cos\delta
\end{aligned}$$

where R1, R2, R3 are rotation angles around the X, Y, and Z axes of the celestial reference frame, respectively, D1, D2, D3 represent the glide parameters, and $\Delta\alpha$ and $\Delta\delta$ are coordinate differences between the studied and the ICRF2 catalogs. All other parameters are relevant to the quadrupolar deformation. The parameters were fitted by weighted least squares to the coordinate difference of the common sources between the catalogs and the references. The covariance (weight) matrix included the a priori covariance information between the provided estimates of the radio source coordinates. A representation of the rotation and glide parameters is displayed in Fig. 3. The standard deviation and chi-squared of the offsets to the reference before and after removal of the systematics are reported in Table 2. Generally, the largest excursion from the ICRF2 shows up for the D3 parameters expressing a poleward displacement of the sources. For Australian solutions, both rotation and glide parameters remain insignificant. Interestingly, the poleward deformation also shows up for the comparison against Gaia but with the reversed sign indicating that the 2016 VLBI catalog deformation lies somewhere between the ICRF2 and Gaia.

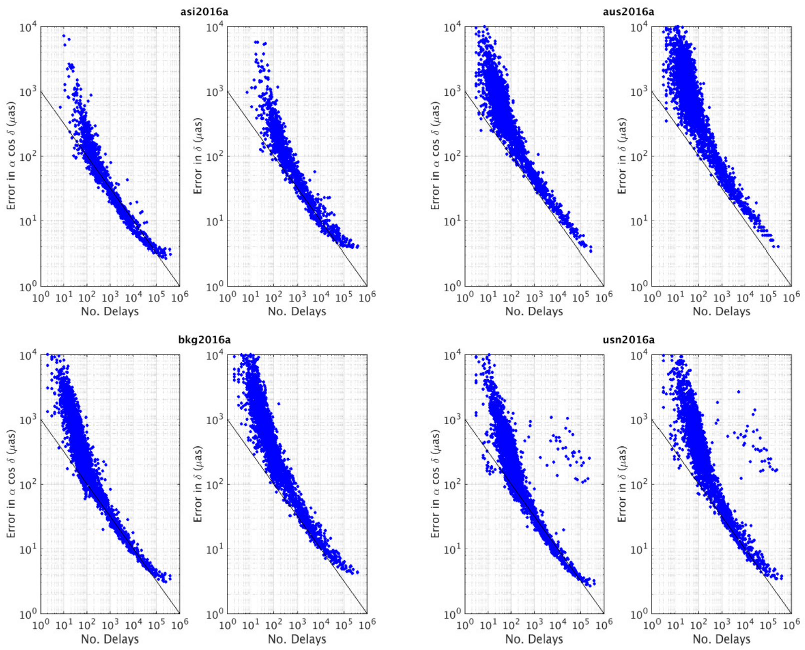

Fig. 2: *The formal error as a function of the number of delays. See text for details.*

Zonal errors In Fig. 4, we plotted the differences in declination between catalogs and the reference averaged in ten bins of declination of equal width between -70° and +70°. The systematics were not removed, so that the differences are direct differences between the catalogs and the reference. Data have been weighted using the total variance coming

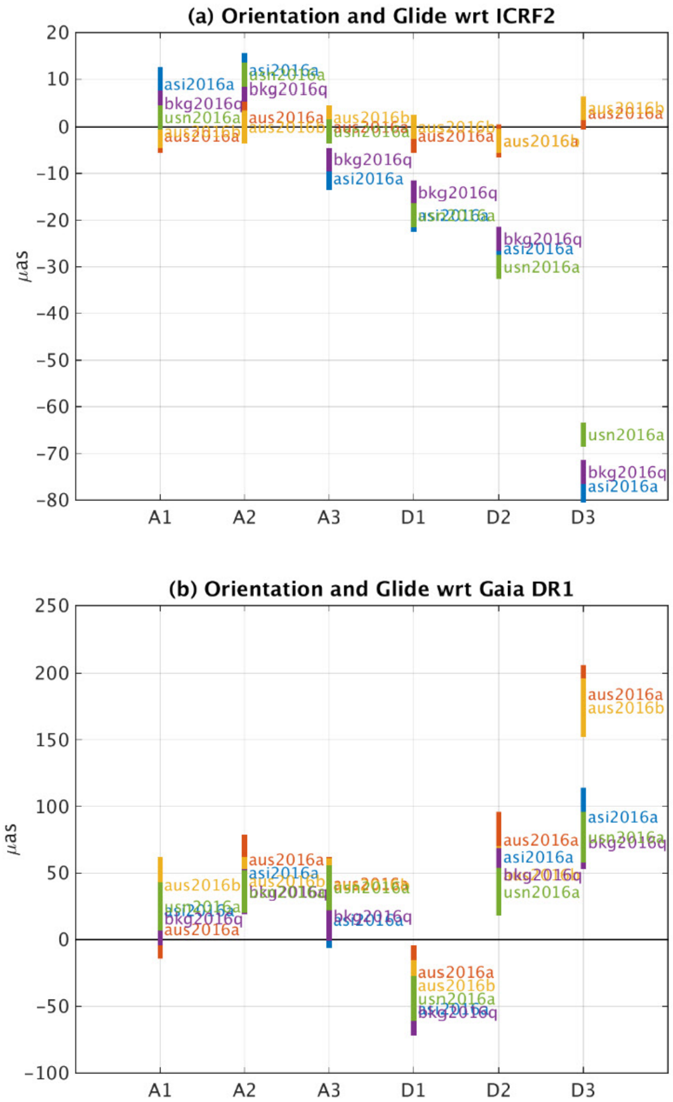

Fig. 3: *The rotation and glide parameters between the catalogs and the reference that are (Left) the ICRF2 and (Right) Gaia DR1. Unit is micro-arcsecond.*

from the errors in the two compared solutions. Comparison against ICRF2 (panel (a)) reveals that the differences are generally increasing in absolute value when going southern except for the Australian solutions, which is consistent with the estimated rotation and glide parameters (Fig. 3). If one consider that (i) zonal errors in VLBI catalogs can be expected because of the network north-south asymmetry and (ii) the Gaia catalog has no zonal error or, at least, smaller than for VLBI, plots of Figs. 3 and 4 can provide insights in how much VLBI catalogs have improved since the ICRF2 from the zonal deformation point of view. Especially, in the (b) panels of the figures, the deformation and declination difference values relevant to Australian solutions are similar to what one would have obtained by comparing the ICRF2 to Gaia. The 2016 ASI, BKG, and USNO solutions appear therefore “closer” to Gaia for D3 and in terms of declination differences.

Table 2: *Crude and residual (i.e., after removal of systematics) differences between catalogs and references (ICRF2 and Gaia DR1). Unit is micro-arcsecond. Values for right ascension, referred to as RA*, are corrected from the cosine of the declination.*

	Differences				Residuals			
	Stdev		Chi2		Stdev		Chi2	
	RA*	Dec	RA*	Dec	RA*	Dec	RA*	Dec
ICRF2								
asi2016a	83	102	0.85	0.91	80	94	0.79	0.78
aus2016a	122	137	0.62	0.57	121	136	0.62	0.57
aus2016b	108	123	0.54	0.51	108	123	0.54	0.51
bkg2016a	89	113	0.44	0.49	87	106	0.42	0.43
usn2016a	96	118	0.47	0.49	93	112	0.44	0.44
Gaia								
asi2016a	363	461	1.88	1.47	357	457	1.82	1.45
aus2016a	537	700	1.59	1.40	532	696	1.57	1.39
aus2016b	519	696	1.59	1.41	516	694	1.57	1.41
bkg2016a	493	627	1.77	1.49	490	624	1.75	1.48
usn2016a	464	570	1.69	1.33	463	567	1.68	1.32

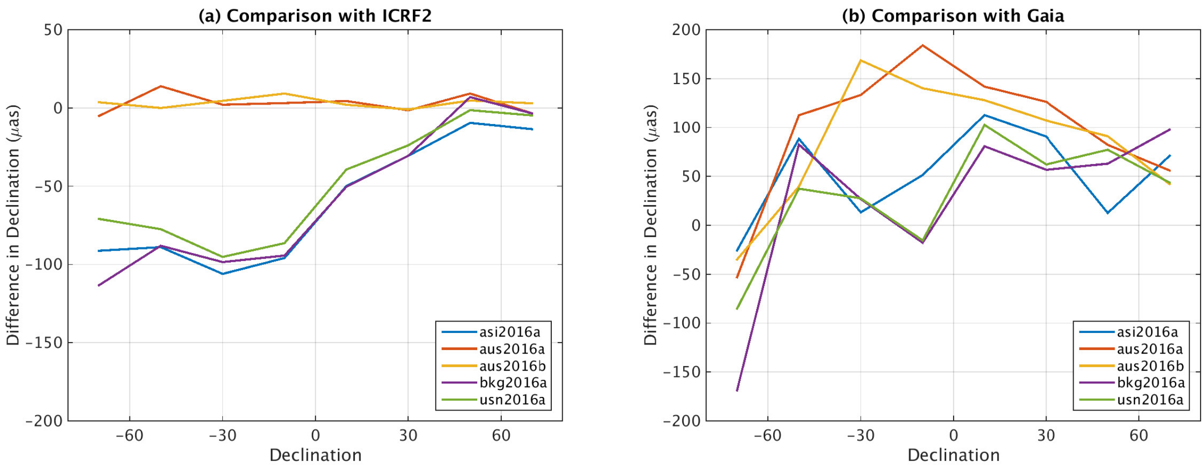

Fig. 4: *Difference in declination between catalogs and the references binned by interval of declination.*

Validation of the Gaia DR1 catalogue for QSOs

Members of the ICRS Center staff belong to the Working Group Package WP944 from CU9 of the Gaia DPAC. Our work was to validate the QSOs from the Gaia catalogue release using external QSO catalogues. In summer 2016, we created and ran our validation tests (VTS) on the QSOs from Gaia DATA RELEASE 1 (GDR1) catalogue before the public release.

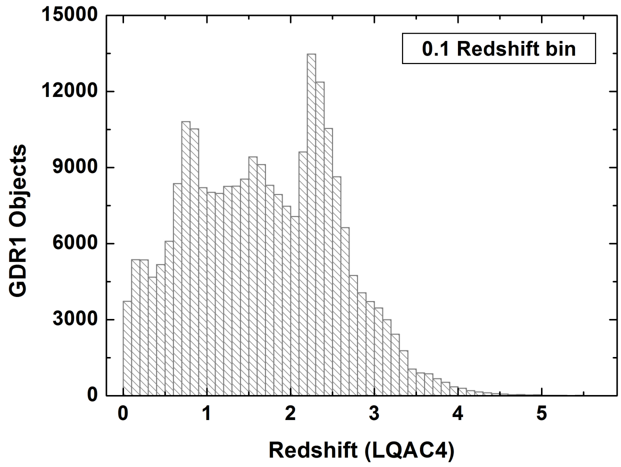

Fig. 5: *Spectroscopic redshift histogram for the LQAC4 quasars found in the GDR1 with a search match radius of 1arcsec. The double peak – at about redshift 0.8 and redshift 2.2 - derive from the domineering number objects from the SDSS, either the classic north galactic cap plus the BOSS surveys.*

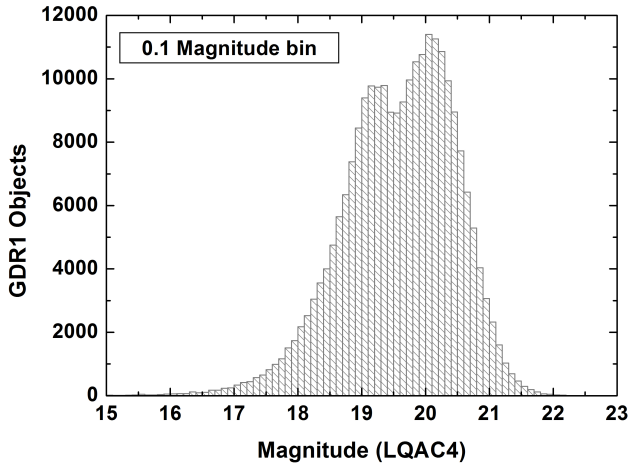

Fig. 6: *Magnitude histogram for the LQAC4 quasars found in the GDR1 with a search match radius of 1arcsec. The magnitudes are from the LQAC4. The double peak – at about magnitude 19.3 and magnitude 20.1 - derive from the domineering number objects from the SDSS, either the classic north galactic cap plus the BOSS surveys.*

Gaia DR1 contains a total of 1,142,679, 769 sources. The astrometric section of Gaia DR1 is built in two populations. The first one concerns the primary sources, which contain positions, parallaxes, and mean proper motions for 2,057,050 of the stars brighter than about magnitude V = 11.5 (about 80% of the total number of stars). This data set, the

Tycho Gaia Astrometric Solution (TGAS), was obtained through the combination of the Gaia observations with the positions of the sources obtained by Hipparcos (ESA 1997) when available, or Tycho-2 (Høg et al. 2000). The second population of the Gaia DR1 concerns the secondary sources, which contain the positions and G magnitudes for 1,140,622,719 sources brighter than magnitude G = 21.

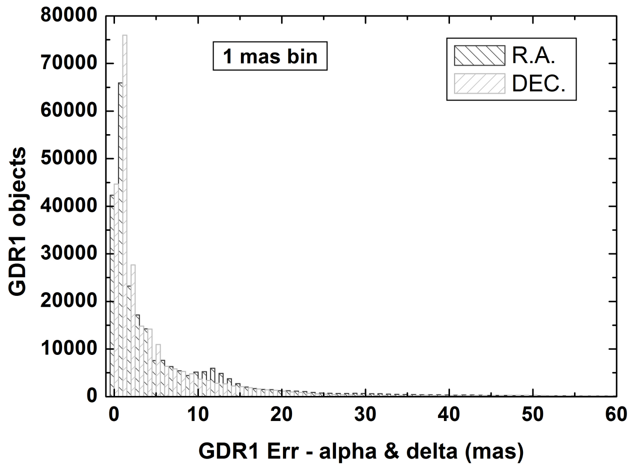

Fig. 7: *Error histogram for the LQAC4 quasars in the GDR1, found using a search match radius of 1 arcsec. The right ascension and declination both follow well the expected distribution. The small departures of one distribution to another are non statistically significant.*

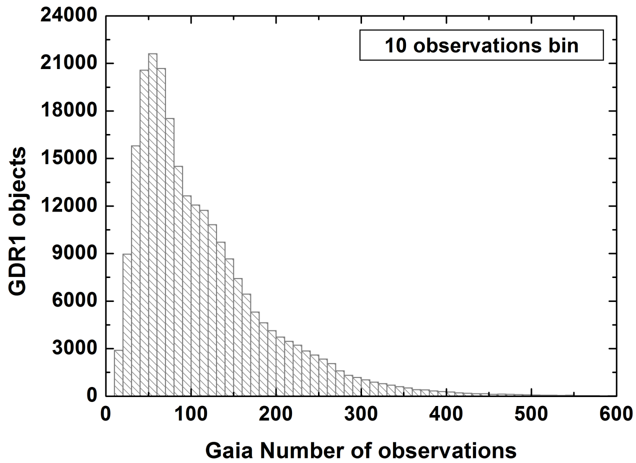

Fig. 8: *Number of observations for the LQAC4 quasars the GDR1, found using a search match radius of 1arcsec. The distribution is as expected from the satellite scanning law.*

We have used the ESAC SVN to run our test written in Java and R languages. The main test (VTS 060_004) was the comparison between the ICRF2 catalogue and the second population of the Gaia DR1 catalogue by a crossmatch position within a 0.1 arcsecond radius. A total of 2,292 ICRF2 quasars were found in the Gaia DR1. No significant rotation versus the ICRF2 was found, but a deformation (glide) lower than 0.2 mas was detected. It should be noted that this deformation is no longer significant if the cross-match radius is increased from 0.1 to 0.5 arcsecond, which adds 15 sources.

The residuals of the position differences normalized using the covariance matrix of both Gaia DR1 and the ICRF2 Rx show too many outliers, that is to say 10% of the sample with a p-value <0.01, i.e. 10 times more than expected and Rx is correlated both with the magnitude and with the number of observations.

In other tests (VTS 60_001 and VTS 60_002) we have verified that QSOs have been correctly observed and identified by Gaia. The first test compares Gaia DR1 QSOs with ground-based quasar compilations: the GIQC (Andrei et al. 2014), the LQAC-3 (Souchay et al. 2015), and the SDSS DR10 (Pâris et al. 2014) catalogues. This check stands for completeness, duplication, and magnitude consistency. While the QSOs were sometimes affected by duplicated sources the filtering seems to have removed them nicely. It was found that 81% of the GIQC, 53% of the LQAC-3, and 11% of the SDSS QSOs are present in the Gaia DR1, a ratio that reaches 93% for the LQAC-3 sources with a magnitude B brighter than 20. These tests results have been described in (Arenou et al., 2017) which accounts for the Gaia Data Release 1 Catalogue Validation.

Analysis of the Gaia GDR1 based on the LQAC-4 catalogue

From 2016 onwards, discovery and studies of quasars have been steadily progressing due mainly to the large synoptic optical surveys (for a recent comprehensive account see Mickaelian, 2016). The Pan-STARRS – a consortium of several institutes, collectively managed by the Pan-STARRS Project Office – lead to a total number of 3 billion sources, among which several hundred thousand of quasars can be matched. For instance, Hernandez et al. (2017) analyzed the light-curves of 104 highly variable quasars. The LSST – also a consortium of several institutes, collectively managed by the LSST Project Office – expects to find out ten million quasars among the several billion observed sources, through selection techniques based on colors, variability properties, and astrometric behavior (Ivezić 2016). This emphasizes the interplay between astrophysics, photometric, and astrometric techniques to characterize quasars and clearly, to the point here, to select those apt to form a Celestial Reference Frame.

The SDSS – a consortium of several institutes, collectively led by the Alfred Sloan Foundation – is the largest contributor of spectroscopically confirmed quasars. On top of that the Large Quasar Astrometric Catalog series (Souchay et al. 2015), now reaching its fourth version LQAC-4 (Gattano et al. 2017) compiles the SDSS quasars plus other confirmed quasars of good astrometric quality. Finally, the Gaia data releases have already started (Lindegren et al. 2016). Although the number of quasars within its final catalog should be smaller than in the previously mentioned surveys, Gaia will provide important features for maybe half a million quasars: above-the-atmosphere observations, full sky coverage, more than one hundred individual measurements spread over 5 years, and remarkable astrometric quality in average as well as for the individual measurements. Although a combination of its own color, astrometry and variability data, has been proven capable of discerning quasars with high confidence, in its first release, GDR1, the quasars were found only by cross-matching with existing quasars catalogs.

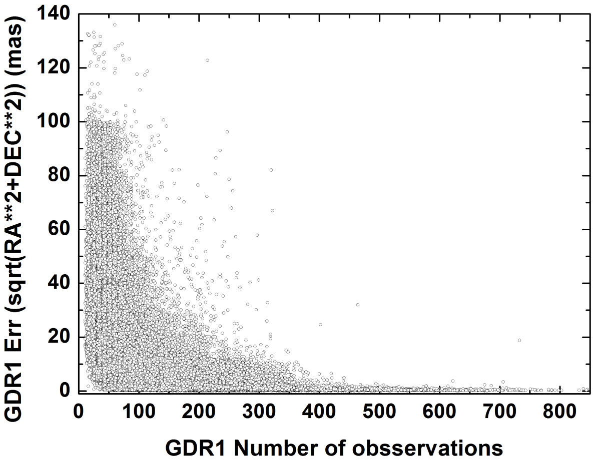

Fig. 9: *GDR1 compound error (quadratic mean from the right ascension and declination errors) according to the number of observations, for the LQAC4 quasars found using a search match radius of 1arcsec. A consequence of the dependence of the errors with the scanning law is highlighted in the text and in Fig. 10.*

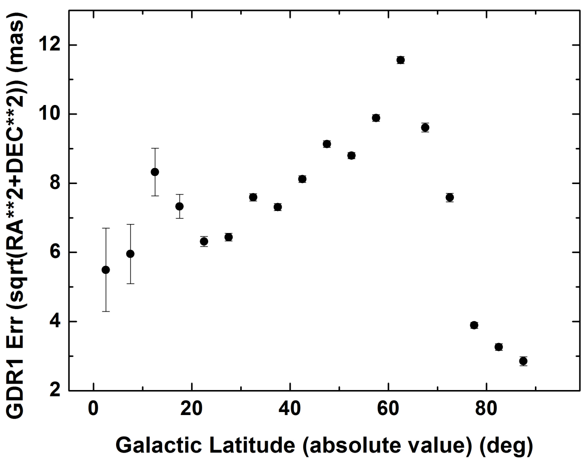

Fig. 10: *Apparent dependence of the GDR1 astrometric error with the galactic latitude, for the LQAC4 quasars found using a search match radius of 1 arcsec. A corresponding dependence appears in declination. They follow from the limited number of observations used to form the GDR1, and of the scanning law. The effect is asymptotic and should be all but vanished in the final Gaia catalogue.*

In the following, we report on the match between the GDR1 and the LQAC4, and present the main results.

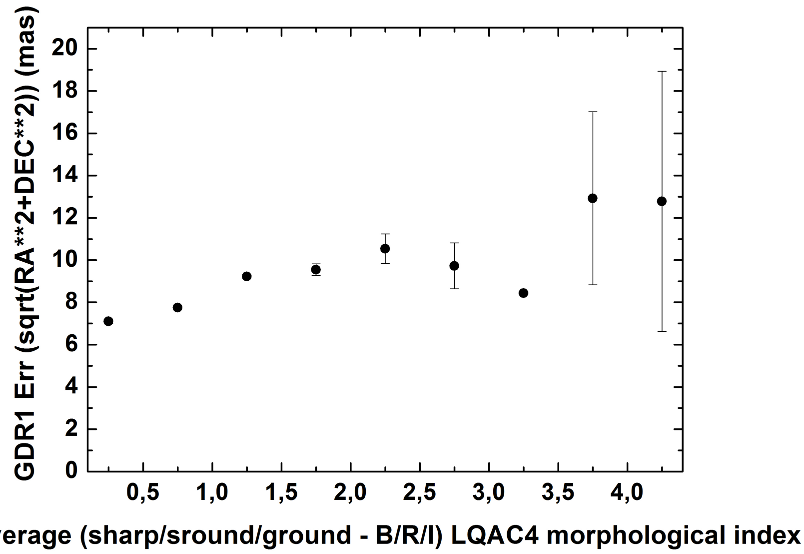

Fig. 11: *Dependence of the GDR1 quasars' astrometric error to the morphological index, obtained from the LQAC4. The main consequences of such dependence are examined in the text.*

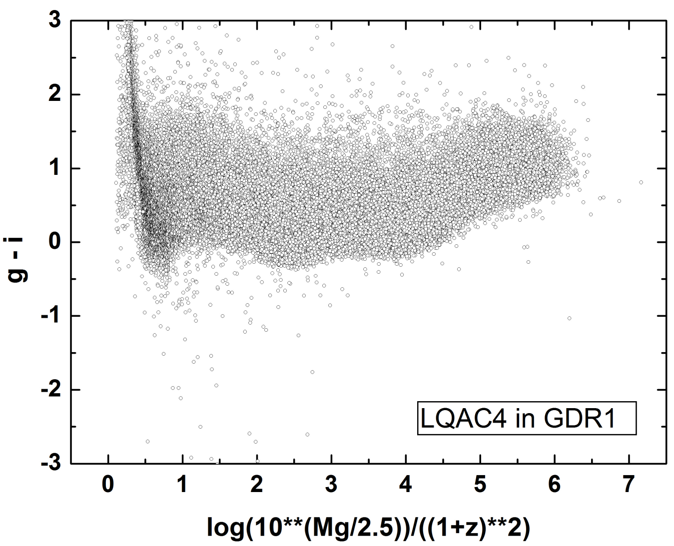

Fig. 12: *Loci of the GDR1 quasars, that is matched to the LQAC4 using a search radius of 1 arcsec, in the color versus magnitude plane. The color is the (g-i) color index taken from the SDSS entries. The magnitude is normalized accounting for the redshift, in order to provide a meaningful comparison to the fainter LQAC4 quasars not found among the GDR1 objects.*

There are 253,444 LQAC-4 quasars found in the GDR1 with a 2 arcsec search radius match. Of these, only 252 LQAC-4 quasars are matched to 2 GDR1 objects and only 1 LQAC-4 quasar is matched to 3 GDR1 objects. Although the matching is thus unambiguous, a more restrictive matching was made using a 1 arcsec radius match. In this case there are 249,071 LQAC-4 quasars found in the GDR1 and no case of double matching within the radius. The mean difference between the GDR1 magnitude and the LQAC-4 (average) magnitude is just -0.03 with a rms of 0.43. Moreover this difference exceeds 3 magnitudes for no more than 471 quasars. In the following, this set of LQAC-4 quasars matched with the GDR1 entries will be quoted as “LQAC4inGDR1”.

The redshift and magnitude distributions are shown in Figures 5 and 6. The double peaks, present in both histograms, derive from the dominant number of objects from the SDSS, either the classic north galactic cap plus the BOSS surveys. The correspondence between the GDR1 G magnitude and the nearest magnitude derived from the LQAC-4 data is also quite well behaved, but note the width around the line of perfect identity, indicating the quasars large photometric variability.

The histograms for the distribution of errors (combined RA and DEC) and the number of observations (transits), as well as the plot of errors versus the number of observations are shown respectively in Figures 7, 8, and 9. They follow what is expected from the mission accuracy goals. It is however worth mentioning that the known dependence of error to the number of transits reflects on larger errors near the galactic plane (but off its poles) and around the equator as can be seen in Fig. 10 with respect to the galactic latitude. The effect, although it may be enhanced by the quasars variability, is asymptotic and will drop at the end of mission. Nevertheless, given the relatively small number of VLBI sources available for the link between the ICRF and the GCRF, and the north-south asymmetry of the former, this issue must be kept under scrutiny.

The morphological indexes presented in the LQAC catalogues series are also included in the Gaia QSO Initial Catalog. Except in a handful of peculiar and very close quasars, the morphological indexes are due to isophotes of the underlying host galaxy. Although most of quasars are stellar-like objects, about 10% of the population present non-negligible apparent morphology on frames taken with ground-based telescopes. Gaia’s astrometry instrument, working free from the atmosphere and flexure disturbances, is apt to be more sensitive than ground-based astrometric instruments. An extended structure – from 100 to 1,000 times fainter than the central source – would give rise to three kinds of disturbances: a larger astrometric error on the centroid because of poorer wings fit; an astrometric jittering due to an asymmetric underlying structure seen along different viewpoints on different with respect to each transit; a poorer fit to the corresponding VLBI-ICRF centroid because of the two previous points. Indeed, Fig. 11 shows a dependence of the GDR1 reported astrometric errors to the ground based derived LQAC-4 morphological indexes.

There are also a large quantity of LQAC-4 sources that do not appear in the GDR1. For these we adopted an exclusion with a search radius of 2 arcsec. Notice that with such a positional limit the number of LQAC-4 objects with defective astrometry is very small. At total 190,201 LQAC-4 objects were not found in the GDR1, and this set will be here termed LQAC4notGDR1. The majority, 128,100 objects have (average) LQAC-4 magnitude beyond 21, therefore they might have been too faint for Gaia detection, at least during the time lapse corresponding to the GDR1. For the sake of comparison just 2.8 % of the LQAC4inGDR1 objects have a magnitude larger than 21.

The average magnitudes <M> and redshift <z> for the LQAC4notGDR1 and LQAC4inGDR1 sets are respectively:

```
LQAC4inGDR1 :  <M> = 19.62 +/-  0.85 ;  <z> = 1.73 +/- 0.88
LQAC4notGDR1:  <M> = 20.56 +/-  1.22 ;  <z> = 1.39 +/- 0.82
```

These values are expected, for dimmer objects are more difficult to be seen by Gaia. But neither the magnitude difference, nor the redshift difference are themselves too large.

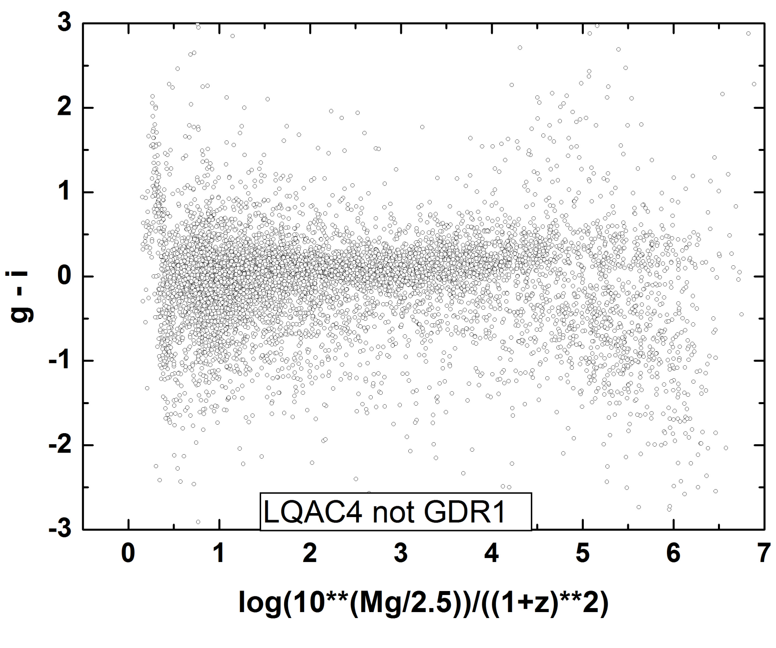

Fig. 13: *Loci of the LQAC4 quasars, not matched to any GDR1 object using an exclusion radius of 2 arcsec, in the color versus magnitude plane. The color is the (g-i) color index taken from the SDSS entries. The magnitude is normalized accounting for the redshift, in order to provide a meaningful comparison to the brighter LQAC4 quasars found among the GDR1 objects*

On the other hand the morphological indexes distributions are indistinguishable in the LQAC4notGDR1 population from the LQAC4inGDR1 one. This is clearly shown in Fig. 11. The relationship between morphological indexes is clear there, but at a level around 10% or 20%, that is not enough to impede the detection of the strong central bright spot.

To progress further we investigated the color distribution. For this we used the (g-i) relative color present in the SDSS, from which most of the quasars of the both sets belong. A color magnitude plane was build. Since the mean magnitude and redshift are different, a reduced magnitude is built as $\log(10^{(M/2.5)})/((1+z)^2)$. Figs. 12 and 13 reveal that the loci of each set is separated in the color/reduced magnitude plane. The detected quasars are redder than the undetected ones. The coating of Gaia's mirror can offer an explanation. Remembering however that most of the undetected quasars are probably too faint, what should perhaps be learnt is that there are classes of quasars that would remain underrepresented even in the very complete Gaia catalog.

Photometric monitoring of quasars with a telescope network

As in the radio domain, it can be reasonably postulated that quasar optical flux variations can alert us to potential changes in their source structure. These changes could have important implications for the position of the target photocenters, together with the evolution in time of these centers, and in parallel have consequences for the link of the reference systems.

In 2016 we used observations made by a set of nine optical telescopes to monitor the magnitude variations of quasars at the same time as Gaia (thanks to the Gaia Observation Forecast Tool). These observations were made in close collaboration with G. Damljanovic from Belgrade Observatory. The telescopes involved were:

- 1.40m and 0.60m telescopes in Vidojevica (Serbia),
- 0.60m and 2.00m Rozhen (Bulgaria),
- 0.60m Belogradchik (Bulgaria),
- LFOA 1.5m (Austria),
- 0.25m TAROT telescopes (France, Chile),
- TJO 0.8m (Spain).

The Allan variances, statistical tools, widely used in the atomic time and frequency community, were adopted to characterize the stability of the magnitude time series with the aim of quantifying the photometric quality of quasars. This method could help to select sources for the link between reference systems and will be the subject of a paper to be published in 2017.

Another program began in 2015 and was pursued in 2016, in collaboration with Z. Malkin from Pulkovo Observatory. It is devoted to the observation, with the TJO, of targets coming from the OCARS catalogue (http://www.gao.spb.ru/english/as/ac_vlbi/). Due to the very large number of targets (>5000), this program will be completed during the year 2017. The goal is to observe a set of targets that have been observed with the radio VLBI techniques but which are not very well known from the optical point of view. In this way, we can put limitations on the magnitudes/variability of the targets and then extend the list of those suitable to the link between the reference systems.

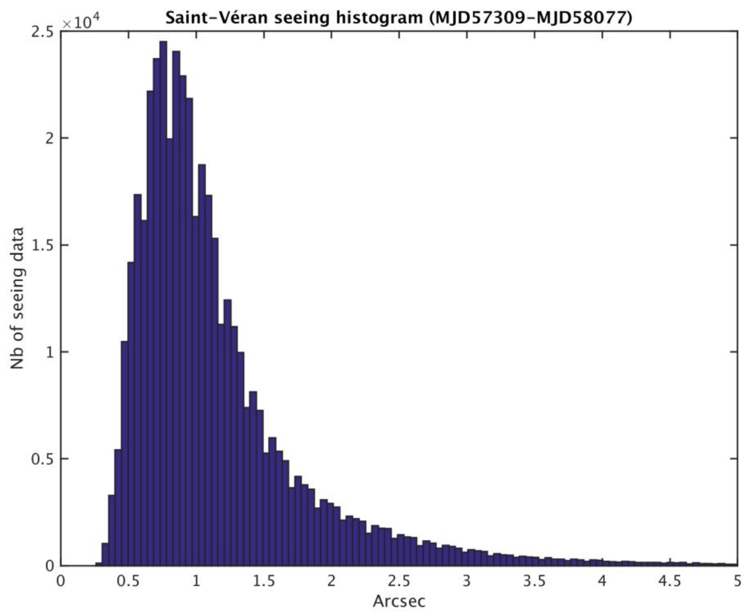

Fig. 14: *Saint-Véran seeing histogram*

The SyRTE department of Paris Observatory plan to build a robotic telescope dedicated to the monitoring of QSO magnitudes. The first part of this project began in 2015 by the choice of a site with a good atmosphere, characterized by its seeing. Saint-Véran (altitude 3000m), in the French Alps, near the Italian border, was chosen to implement a site seeing monitoring campaign (http://stveran.obspm.fr/index.php?page=statistiques). It has been demonstrated in 2016 (see Figure 14) that the median value of the seeing is 1" (mode seeing is 0.7") which made this site a very good one (see Figure 15), probably one of the best in Europe. In the second step of this project, the SyRTE laboratory proposed to robotize a test telescope (0.50m) already on site since 2015. This part of the project will be achieved in 2017.

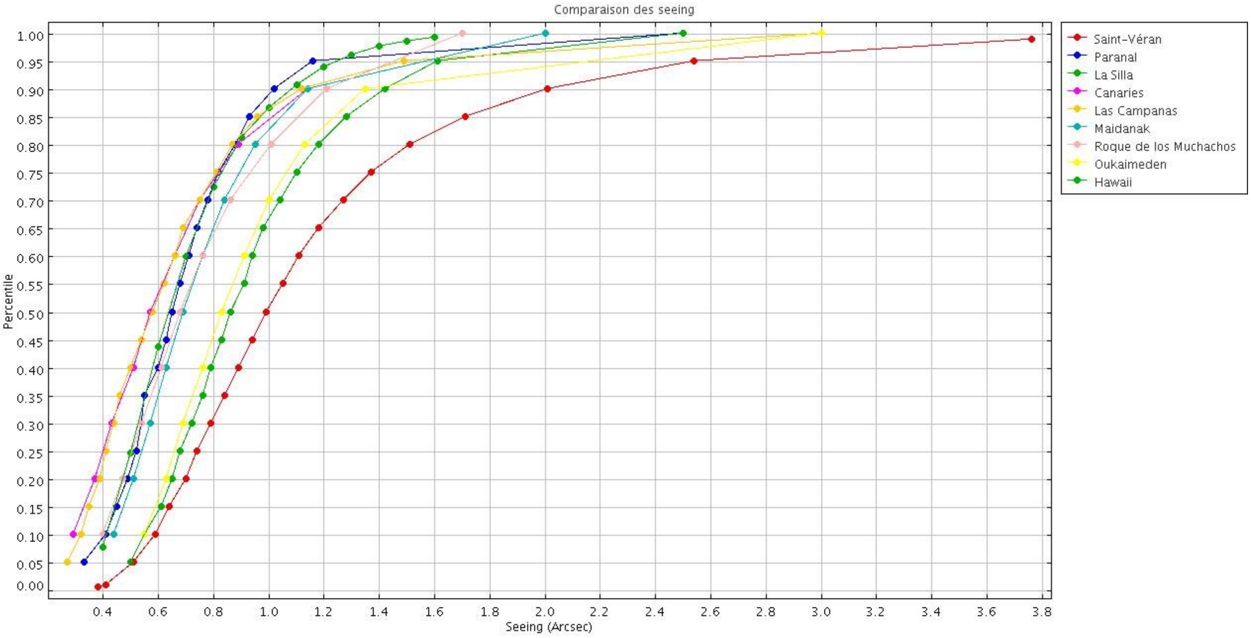

Fig. 15: *Cumulative distribution of the seeing for Saint-Véran and for the best sites in the world. The curve for Hawaii is derived from https://www.subarutelescope.org/Observing/Telescope/ImageQuality/Seeing/ and the other ones from: Frogel, J. A., 2002. Image quality at selected astronomical observatories V3.0. A memo prepared by Jay A. Frogel for the SNAP project at the Lawrence Berkeley National Laboratory, 1 February 2002.*

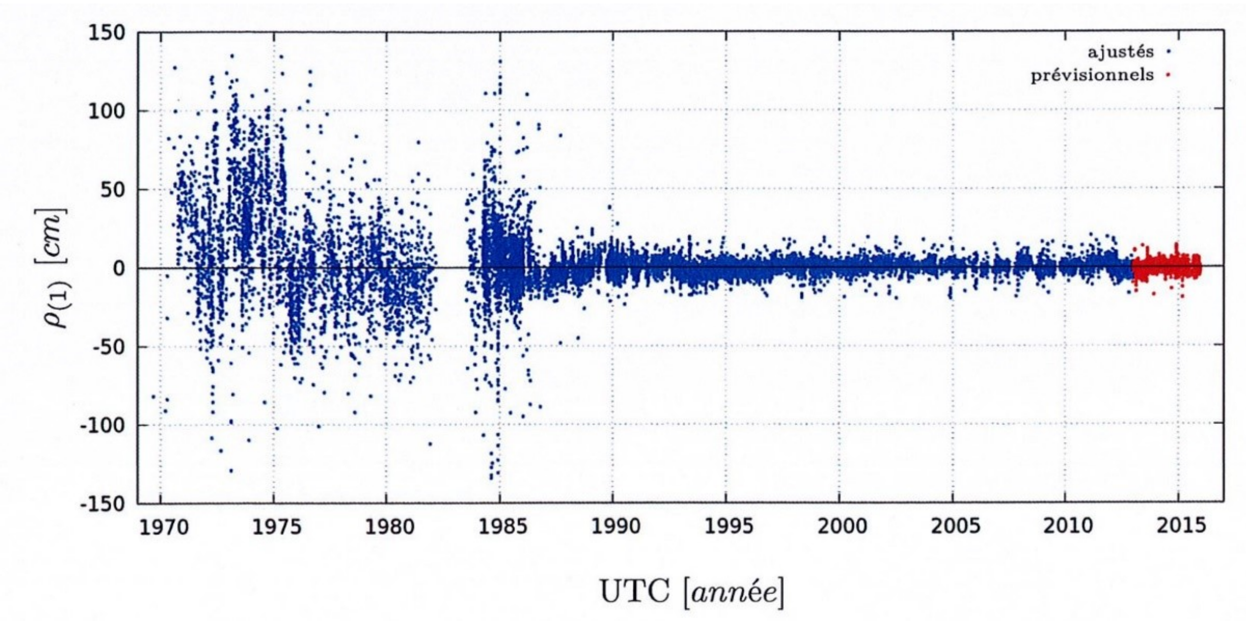

Fig. 16: *Amplitude of the O–C residuals calculated starting from the reduction software CAROLL, by using the ELPN series. In blue the observations used to make the adjustments. In red the observations not used for adjustment.*

Lunar Laser ranging (LLR) activities with POLAC

POLAC is the acronym of "Paris Observatory Lunar Analysis Center". It represents one of the four LLR analysis centers reckoned by the ILRS (International Laser Ranging Service). In addition of its mission of collecting, filtering and distributing LLR data, it works continuously in close collaboration with the Laser ranging station Méo of the OCA (Observatoire de la Côte d'Azur) by furnishing in a daily basis the predictions of the LLR observations and a regular validation of the normal points. In addition, since 2013, it works with the SLR component of the GRGS (Groupe de Recherche en Géodésie Spatiale).

Table 3: *Mean values μ and standard deviation σ (in meter), of the residuals obtained with ELPN for each LLR station. The numbers N and Ne represent respectively the total number of observations and the number of observations eliminated, for each station.*

Stations LLR $\{l\}$	Période	$N_{\{l\}}$	$Ne_{\{l\}}$	$\mu_{\{l\}}$ $[m]$	$\sigma_{\{l\}}$ $[m]$
McDonald 2.7m	1969-1985	3516	88	0.094	0.350
McDonald MLRS1	1983-1988	573	58	0.003	0.351
McDonald MLRS2	1988-2013	3284	386	0.006	0.097
Grasse Rubis	1984-1986	1182	6	0.056	0.176
Grasse Yag	1987-2005	8313	11	-0.004	0.045
Grasse MeO	2009-2013	993	6	-0.002	0.036
Haleakala	1984-1990	757	13	-0.004	0.101
Matera	2003-2013	79	11	-0.017	0.130
Apache-point	2006-2013	1806	8	0.001	0.038
Totalité	1969-2013	20503	587	-	-

The works achieved by POLAC in 2016 consisted of:

- Realization and the maintenance of the web service POLAC http://polac.obspm.fr/PaV which enables to the LLR observational team to prepare their laser shots on the lunar reflectors and to check the validity of their observations.
- Annual up-date of the LLR observations done at McDonald, Grasse, Haleakala, Apache Point and Matera since 1969 and coming from 5 different database with 4 different formats.
- Construction of lunar tables including the libration, to insert the LLR component into the multi-technique software GINS in order to product the parameters related to the EOP and to the Celestial reference Frames.
- Analysis of the ELP (Éphéméride Lunaire Parisienne) series by identifying their differences with the numerical ephemerides DExxx

and INPOPx, as well as the limits of these semi-analytical solutions (convergence and truncature problems, effects of uncertainties on physical parameters etc. . .)

In 2016, efforts have been made to reduce the disadvantages above by following two axes of investigation:

- The characterization of the limits of precision of the semi-analytical series ELPs by the intermediary of a rigorous analysis of the amplitude of the uncertainty of each underlying effect. For this purpose the ELP's series are compared with the results of numerical integration of the differential equations they include.
- The replacement of some of the ELP's series by numerical counterparts (when the series converge too slowly).

Moreover in the frame of these activities an alternative theory to the general relativity was tested, whose formalism is called SME (Standard-Model Extension). This theory is based on a parametrization of all the possible violations of the Lorentz symmetry. Thus the new lunar ephemerides, called ELPN, was implemented by taking into account the SME.

Fig. 16 represents the amplitude of the LLR O–C residuals calculated starting from the reduction software CAROLL by using ELPN. Finally, Table 3 shows the mean value and the standard deviation of the residuals obtained with ELPN from the various LLR stations.

USNO ICRS Center Activities During 2016

USNO concentrated on four primary areas of work in support of maintenance and improvement of the Celestial Reference Frame: (1) support to the ICRF3 working group, (2) processing of previously taken URAT Northern Hemisphere data, (3) operation of UBAD in the Northern and URAT in the Southern Hemisphere to collect bright star data, and (4) ingest and assessment of the Gaia data as a Gaia Affiliated Data Center (ADC).

ICRF3

USNO participated as a member of the IAU-sanctioned ICRF3 working group. Work included support for the execution of and analysis of the VCS-II S/X band observing campaign (see Gordon et al. 2016), and support for X/Ka band observations as candidates for inclusion in ICRF3.

URAT Parallax Catalog

The 2016 initial Gaia data release (DR1, see following discussion) included the "TGAS" catalog, which consisted of approximately 2 million stars with the full set of five astrometric parameters. The remaining ∼99.8% of the DR1 release were sources with positions (RA, DEC) only. In order to address this gap in proper motions, USNO released the URAT Parallax Catalog (UPC), a catalog of 112,177 parallaxes covering the magnitude range 6.56 to 16.93 in the URAT band-pass north of -12.752 deg declination, based on the URAT1 and follow-on observations (see Zacharias et al., 2015 for a discussion of URAT1). The UPC includes 56k parallaxes recovered from Hipparcos, and 59k new parallaxes.

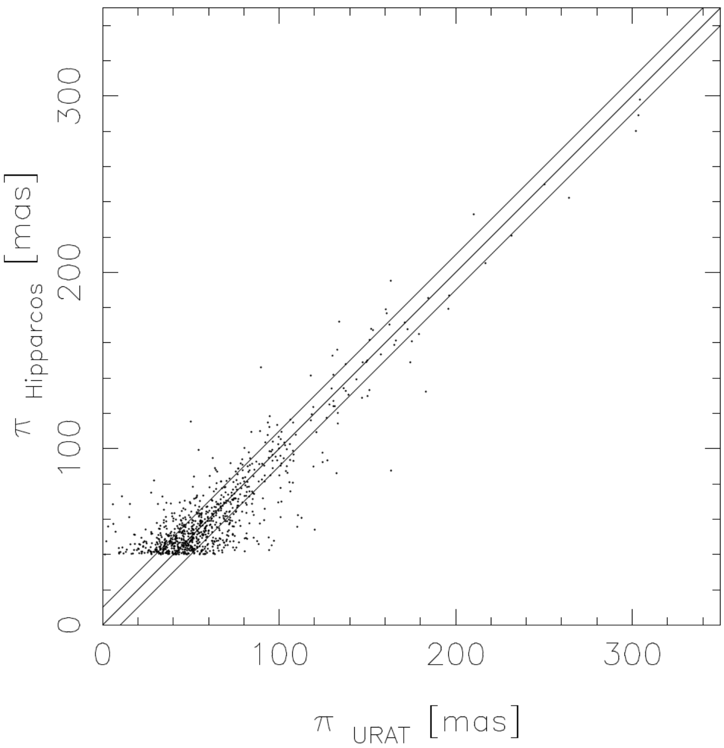

Fig. 17: *Parallax comparison between URAT and the Hipparcos 25 pc sample north of DEC = -10 deg. The center line represents perfect agreement while the outer lines show a ± 10 milliarcsecond (mas) difference.*

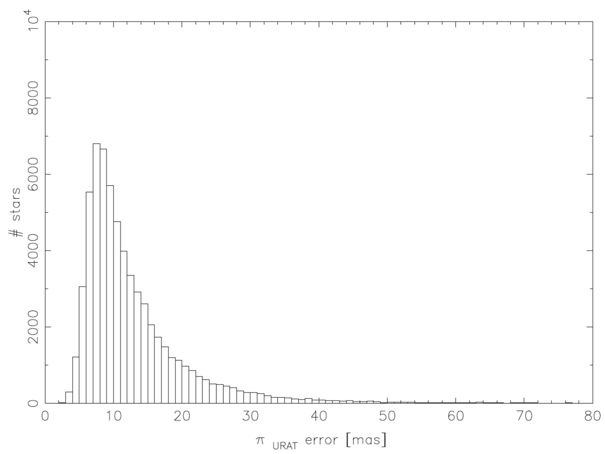

Fig. 18: *Histogram of URAT parallax errors for Hipparcos same north of DEC = -10 deg.*

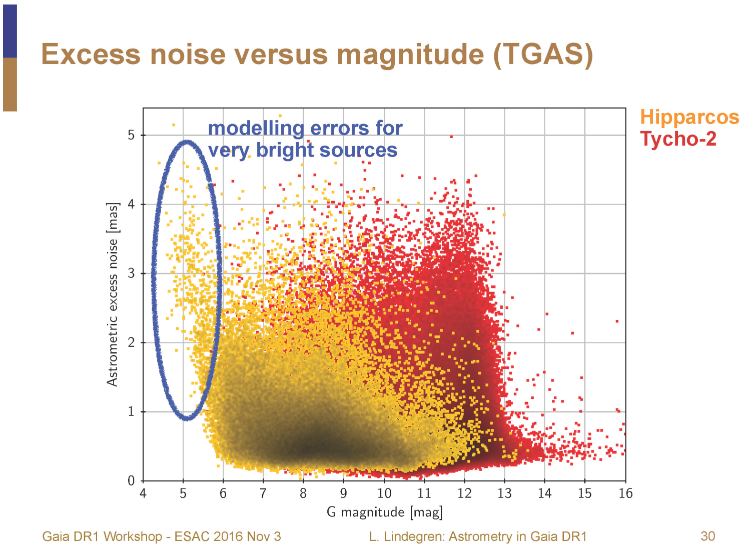

Fig. 19: *Gaia DR1 bright star results. Stars brighter than about G = 6 suffer from significant "astrometric noise". There is currently (i.e., DR1) no authoritative method for measuring bright sources. Results are from the Gaia DR1 workshop.*

The UPC contains 58,677 URAT parallaxes which have a match to either of those catalogs without implementing any extra cuts. For the stars with no prior published parallax, a set of stringent cuts to reduce possible erroneous parallaxes was implemented, resulting in over 53,000 new trigonometric parallaxes from URAT data alone with a high level of confidence. The average parallax precision is 10.8 mas and 4.3 mas for stars having a known parallax and stars without a prior known parallax respectively (see Figs. 17, 18) (Finch & Zacharias 2016a; Finch & Zacharias 2016b). This is the largest catalog of high-accuracy parallaxes released since Hipparcos, and will be definitive until superseded by Gaia DR2.

URAT Southern Hemisphere Bright Star Survey

The Gaia focal plane is configured in such a way as to saturate at G=12 under normal observing conditions. The Gaia focal plane includes "bright star modes" that allow it to get up to G $\sim$ 5–6 before these modes are saturated. As shown in Figure 19, the Gaia DR1 results show large levels of "astrometric noise" for sources brighter than about G=6. The Gaia data processing team is currently looking at approaches to extending the Gaia results to the brightest stars in the sky, but there is currently no clear method for delivering high accuracy results for the brightest stars in the sky.

In order to address this gap in the optical reference frame, USNO has been operating the UBAD survey on its 61" (1.55 m) Strand astrometric telescope located at Flagstaff Station in Arizona for the Northern Hemisphere, and deployed the URAT 8" telescope to Cerro Tololo Interamerican Observatory (CTIO) in October 2015 (see Fig. 20). URAT was modified from its Northern Hemisphere configuration by adding an ND +4.5 spot to one of the detectors, and operating in aperture grating mode (another 4.5 magnitudes of attenuation) for the entire year. Both systems (UBAD and URAT configured for bright stars) are able to observe the brightest stars in the sky (on the bright end), and Gaia stars on the faint end. During data processing and reduction, Gaia results will be used for the reference frame against which the UBAD and URAT data are located with high accuracy. Figure 21 shows the southern hemisphere coverage through the end of 2016.

It is anticipated that the bright star work will conclude in 2018 in time to supplement the Gaia DR2 catalog. At that point, an assessment will be made as to the availability of quality of the Gaia bright star data (and thus, the necessity for USNO to continue to observe and process bright stars for astrometry and photometry.

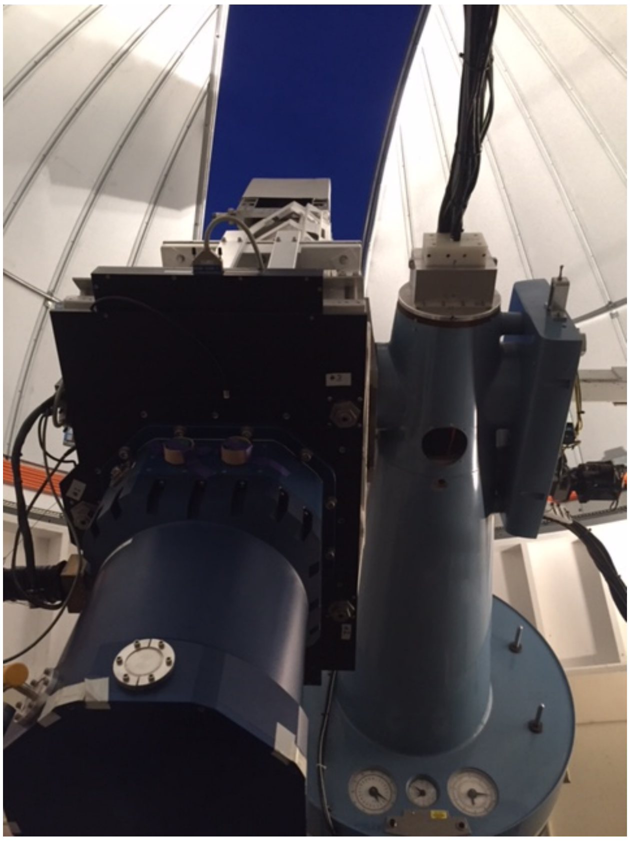

Fig. 20: *USNO Robotic Astrometric Telescope (URAT) deployed to and operating at Cerro Tololo Interamerican Observatory (CTIO) during 2016. URAT is being operating with both a full aperture grating and a neutral density spot that allows it to observe all the brightest stars in the Southern Hemisphere, up to a declination of DEC $\sim$ +25 deg*

Ingest and Assessment of Gaia DR1 Data

USNO received the Gaia DR1 data as one of Gaia's Affiliated Data Centers (ADCs) in the US. The DR1 data was ingested and integrated into USNO's Celestial Reference Frame Database (CDB), where it is stored,

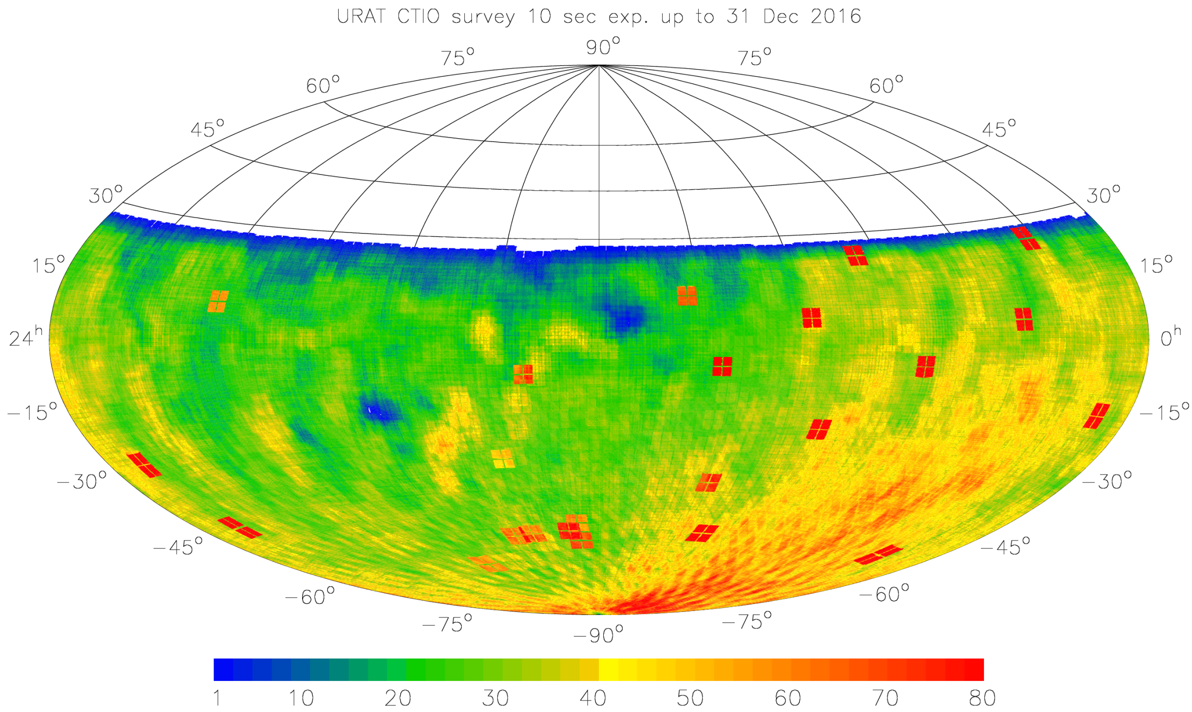

Fig. 21: *URAT Southern Hemisphere coverage through 31 December 2016. Scale along bottom indicates number of times location in sky has been observed. The visible red pattern is the projection of the focal plane on the sky. The identifiable patches that have been observed the most are locations of very bright stars that require dedicated pointings.*

along with data from numerous other programs, missions and catalogs, including Hipparcos, Tycho-2, UCAC4, URAT1, URAT2, Pan-STARRs 1, 2MASS, LQAC, WISE, MIRAGN, and ICRF2. The CDB supports source correlation and analysis across multiple input catalogs, wavelength and magnitude regimes. It is currently used internally at USNO, but may be made available in some form to the public in the future. The Gaia DR1 release immediately became the core, authoritative component of the CDB. Gaia data were validated as authoritative for optical sources from magnitude 6–20.7. Additional work will continue in 2017 in terms of validation of Gaia data and use of Gaia data along with other sources of data (for example, radio and IR positions and luminosities) in order to maintain and improve the overall celestial reference frame across all spectral wavelengths.

References

Andrei, H.; Antón, S.; Taris, F.; et al., 2014, “The Gaia Initial Quasar Catalog”, Proceedings of the Journées 2013 “Systèmes de référence spatio-temporels”: Scientific developments from highly accurate space-time reference systems, Observatoire de Paris, 16–18 September 2013, Edited by Nicole Capitaine, ISBN 978-2-901057-69-7, p. 84–87

Arenou, F.; Luri, X.; Babusiaux, C.; et al., 2017, “Gaia Data Release 1. Catalogue validation”, A&A, 599, 50

Fey, A.; Gordon, D.; Jacobs, C.; Ma, C.; Gaume, R.; Arias, E.; Bianco, G.; Boboltz, D.; B´ockmann, S.; Bolotin, S.; et al., 2015, “The Second Realization of the International Celestial Reference Frame By Very Long Baseline Interferometry”, AJ, 150, 58

Finch, C.T.; Zacharias, N., 2016, “The URAT Parallax Catalog”, VizieR Online Data Catalog, 1333

Finch, C.T.; Zacharias, N., 2016, “Parallax Results from URAT Epoch Data”, AJ, 151, 160

Gattano, C.; Andrei, A.H.; Coelho, B.; et al., 2017, “The fourth release of the Large Quasar astrometric Catalogue”, accepted in A&A

Høg, E.; Fabricius, C.; Makarov, V. V.; Urban, S.; Corbin, T.; Wycoff, G.; Bastian, U.; Schwekendiek, P.; Wicenec, A., 2000, “The Tycho-2 catalogue of the 2.5 million brightest stars”, A&A, 355, 27

Lindegren, L.; Lammers, U.; Bastian, U.; et al., 2016, “Gaia Data Release 1. Astrometry: one billion positions, two million proper motions and parallaxes”, A&A, 595, 4

Mickaelian, A.M., 2016, “Astronomical surveys and big data”, Baltic Astronomy, 25, 75

Mignard, F.; Klioner, S., 2012, “Analysis of astrometric catalogues with vector spherical harmonics”, A&A 547, A59

Mignard, F.; Klioner, S.; Lindegren, L.; Bastian, U.; Bombrun, A.; Hernandez, J.; Hobbs, D.; Lammers, U.; Michalik, D.; Ramos-Lerate, M.; Biermann, M.; Butkevich, A.; Comoretto, G.; Joliet, E.; Holl, B.; Hutton, A.; Parsons, P.; Steidelmüller, H.; Andrei, A.; Bourda, G.; Charlot, P., 2016, “Gaia data release 1 - reference frame and optical properties of ICRF sources”, A&A 595:A5, DOI 10.1051/0004-6361/201629534

Pâris, Isabelle; Petitjean, Patrick; Aubourg, Éric; et al., 2014, “The Sloan Digital Sky Survey quasar catalog: tenth data release”, A&A, 563, 54

Souchay, J.; Andrei, A. H.; Barache, C.; Kalewicz, T.; Gattano, C.; Coelho, B.; Taris, F.; Bouquillon, S.; Becker, O., 2015, “The third release of the Large Quasar Astrometric Catalog (LQAC-3): a compilation of 321 957 objects”, A&A, 583, 75

Zacharias, N.; Finch, C.; Subasavage, J.; et al., 2015, “The First U.S. Naval Observatory Robotic Astrometric Telescope Catalog”, AJ, 150, id. 101

Bryan Dorland, Jean Souchay, Alexandre Andrei, E. Felicitas Arias,
Christophe Barache, Sébastien Bouquillon, Alan Fey,
Sébastien Lambert, François Taris, Norbert Zacharias